Slow deterministic vector rogue waves

S. V. Sergeyev*[a], S. A. Kolpakov[a], Ch. Mou[a], G. Jacobsen[b], S. Popov[c], V. Kalashnikov[a]

[a] AIPT, Aston University, B4 7ET, Birmingham, UK [b] Acreo, Electrum 236, SE – 16440, Kista, Sweden [c] Royal Institute of Technology, SE – 1640, Stockholm, Sweden

Correspondent author: s.sergeyev@aston.ac.uk

ABSTRACT

For an erbium-doped fiber laser mode-locked by carbon nanotubes, we demonstrate experimentally and theoretically a new type of the vector rogue waves emerging as a result of the chaotic evolution of the trajectories between two orthogonal states of polarization on the Poincare sphere. In terms of fluctuation induced phenomena, by tuning polarization controller for the pump wave and in-cavity polarization controller, we are able to control the Kramers time, i.e. the residence time of the trajectory in vicinity of each orthogonal state of polarization, and so can cause the rare events satisfying rogue wave criteria and having the form of transitions from the state with the long residence time to the state with a short residence time.

Keywords: rogue waves, fiber lasers, polarization dynamics, mode–locking

1. INTRODUCTION

Rogue wave (RWs) as a concept has been initially introduced in oceanography to describe giant waves with amplitudes that are much larger than an average and so, despite the low probability of emergence, resulting in destructive impact in nature and society [1-7]. The main obstacles in modeling and predicting rogue waves is in the scarcity of events and the inability to perform full-scale experiments to cause rogue waves to appear in real-world scenarios such as financial markets, power grids, oceans, human brains (epileptic seizures) etc. [1-5]. In this context, mode-locked lasers (MLL) are perfect test bed systems to study RWs origin and techniques of mitigation with potential to apply results beyond the scope of photonics [8-12]. The femtosecond/picosecond pulsewidth range and MHz/GHz repetition rate of pulses in MLL provides an opportunity to observe more data on rogue waves in the form of bunches of noise-like pulses (soliton rain) in the short time frame and under laboratory-controlled conditions [8-12]. It has been found that RWs are emerging in MLL as a result of interaction of pulses (dissipative solitons) through their tails overlapping or through the dispersive waves [8-12]. Such interaction is accompanied by recirculation of pulses in a ring cavity and so results in coupling enhancement and creating chaotic bunching at the time scales shorter than a round-trip time [8-12]. In view of such interaction depends on the cavity parameters, tuning such parameters enabled control of RWs statistics [8].

Unlike the previous study of RWs in MLL [8-12], we reveal theoretically and experimentally a new type of interaction that is based on the coherent coupling of the orthogonal states of polarization (SOPs) in the cavity and leading to the emergence of slow rogue waves. These slow rogue waves (SRWS) take the form of chaotic transitions between orthogonal SOPS at the time scale of hundreds round trips. We demonstrate control of the rogue wave's statistics including RWs suppression and enhancement based on tuning polarization controller for the pump wave and in-cavity polarization controller. In terms of the fluctuation induced escape (FIE) concept [13-16], this type of RWs harnessing means a transformation of the double-well potential landscape to activate polarization instability-driven trajectory escape from the state with the long residence time of trajectories in the vicinity of this state to the state with a short residence time.

Real-time Measurements, Rogue Events, and Emerging Applications, edited by Bahram Jalali, Sergei K. Turitsyn, Daniel R. Solli, John M. Dudley, Proc. of SPIE Vol. 9732, 97320K · © 2016 SPIE · CCC code: 0277-786X/16/$18 · doi: 10.1117/12.2211364

2. THE EXPERIMENTAL SETUP

The schematic diagram of the laser and the pulse train are illustrated in Figure 1.The laser cavity comprises 1.1m of erbium-doped fiber (EDF) which is used as the amplifying element and has absorption of 80dB/m at 1530nm. Moreover, the cavity has 1.22m of *OFS-980* fiber and 6.4m of *SMF 28* fiber. The whole cavity length, including the length of the carbon nanotube (CNT) holder, was measured to be 8.8 meters. The CNT was used as a saturable absorber. The fiber isolator labeled with the abbreviation OISO in the left side of Figure 1 was used to provide unidirectional lasing. For the pump we use a 975nm laser diode with a maximum output power of 300mW; this diode was coupled to the cavity via 980/1550 wavelength division multiplexer (WDM). The fused fiber coupler with the ratio of 70:30 ("OUTPUT C" in Figure 1) was used to direct part of the signal power out of the cavity to the detector. Two polarization controllers (POC1 and POC2) were used to control the state of polarization of the pump wave and the birefringence.

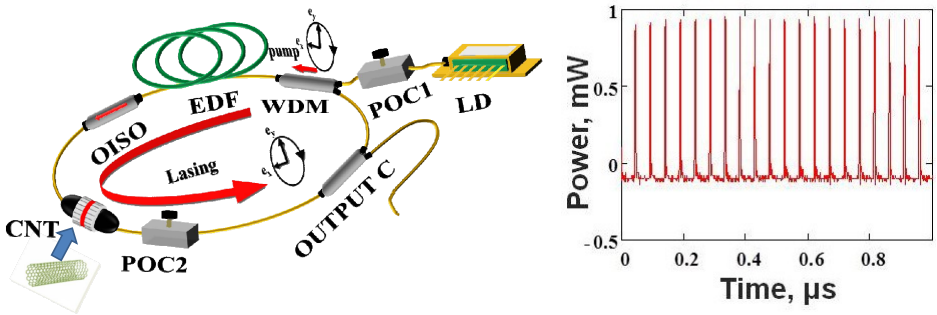

Figure 1. The schematic diagram of the laser (on the left) and the pulse train (on the right).

The polarimeter (*Thorlabs IPM5300)* was mounted on a chassis (*Thorlabs TXP – 5016)* and adjusted to have a 1 μs resolution and a total temporal length of the sample of 1 ms (1024 points per measurement). This polarimeter was used to measure the normalized Stokes parameters s_1, s_2, s_3, the degree of polarization (DOP) and the power of the signal. The polarimeter integrated the signal over ~20 roundtrips to assure the observation of slow optical rogue wave patterns (SORW). The laser signal was measured using a *UDP–15 –IR–2FC* detector with a bandwidth of 17 GHz; the electric signal from the detector was recorded with a *Tektronix DPO7254 – 2.5 GHz* oscilloscope. The switching between the available regimes was done by changing the angle between the control levers of POC1 and POC2. During this set of experiments both POCs were tuned to assure the regime of SORW generation and remained fixed.

3. THE THEORETICAL MODEL

3.1 The system of equations

Evolution of the laser SOPs and population of the first excited level in Er^{3+} doped active medium has been modeled by using the equations developed by Sergeyev et al. [17, 18]:

$$\frac{d|u|}{dt}=\left(\frac{\alpha_1(f_1+f_2)}{1+\Delta^2}-\alpha_2\right)|u|+\frac{\alpha_1 f_3}{1+\Delta^2}|v|\cos(\Delta\phi)-\frac{\alpha_1 f_3\Delta}{1+\Delta^2}|v|\sin(\Delta\phi)+\frac{2\gamma}{3}|v|^2|u|\sin(2\Delta\phi)-F(|u|,|v|),$$

$$\frac{d|v|}{dt}=\left(\frac{\alpha_1(f_1-f_2)}{1+\Delta^2}-\alpha_2\right)|v|+\frac{\alpha_1 f_3}{1+\Delta^2}|u|\cos(\Delta\phi)+\frac{\alpha_1 f_3\Delta}{1+\Delta^2}|u|\sin(\Delta\phi)-\frac{2\gamma}{3}|u|^2|v|\sin(2\Delta\phi)-F(|u|,|v|)$$

$$\frac{df_1}{dt}=\varepsilon\left[\frac{(\chi-1)I_p}{2}-1-\left(1+\frac{I_p}{2}+d_1S_0\right)f_1-\left(d_1S_1+\frac{I_p}{2}\frac{(1-\delta^2)}{(1+\delta^2)}\right)f_2-d_1S_2f_3\right],$$

$$\frac{df_2}{dt}=\varepsilon\left[\frac{(1-\delta^2)}{(1+\delta^2)}\frac{I_p(\chi-1)}{4}-\left(\frac{I_p}{2}+1+d_1S_0\right)f_2-\left(\frac{(1-\delta^2)}{(1+\delta^2)}\frac{I_p}{2}+d_1S_1\right)\frac{f_1}{2}\right],$$

$$\frac{df_3}{dt}=-\varepsilon\left[\frac{d_1S_2f_1}{2}+\left(\frac{I_p}{2}+1+d_1S_0\right)f_3\right],\frac{d\Delta\phi}{dt}=\Delta\Omega+K_{NL}\sin^2(\Delta\phi)+K_s\sin(\Delta\phi)+K_{as}\cos(\Delta\phi),$$

$$\Delta\Omega=\frac{2\alpha_1 f_2\Delta}{1+\Delta^2}-2\beta,K_{NL}=\frac{\gamma LI_{ss}}{6}\left(|v|^2-|u|^2\right),K_s=-\frac{2\left(|v|^2+|u|^2\right)}{|u||v|}\frac{\alpha_1 f_3}{(1+\Delta^2)},K_{as}=\frac{2\left(|v|^2-|u|^2\right)}{|u||v|}\frac{\alpha_1 f_3\Delta}{(1+\Delta^2)},$$

$$F(|u|,|v|)=\frac{\alpha_0}{\pi}\left(1-\sqrt{\frac{\alpha_s\left(|u|^2+|v|^2\right)}{1+\alpha_s\left(|u|^2+|v|^2\right)}}\arctan\left(\sqrt{\frac{\alpha_s\left(|u|^2+|v|^2\right)}{1+\alpha_s\left(|u|^2+|v|^2\right)}}\right)\right). \tag{1}$$

Here time is normalized to the round trip time; $/u/,\ /v/$ are amplitudes of two orthogonal linearly polarized modes, (pump and lasing powers (I_p and $/u/^2,\ /v/^2$) are normalized to the corresponding saturation powers I_{ps} and I_{ss} [17, 18]; α_1 is the total absorption of erbium ions at the lasing wavelength, α_0 is CNT absorption coefficients at the lasing wavelength, α_3 is the ratio of saturation powers for CNT and erbium doped fiber, α_2 is the total insertion losses in cavity, β is the birefringence strength ($2\beta=2\pi L/L_b$, L_b is the beat length); $\gamma=\gamma_k LI_{ss}$ (γ_k is the Kerr coupling constant), δ is the ellipticity of the pump wave, $\varepsilon=\tau_R/\tau_{Er}$ is the ratio of the round-trip time τ_R to the lifetime of erbium ions at the first excited level τ_{Er}; $\chi=(\sigma_a^{(L)}+\sigma_e^{(L)})/\sigma_a^{(L)}$, $\sigma_a^{(L)}$ and $\sigma_e^{(L)}$are absorption and emission cross sections at the lasing wavelength; Δ is the detuning of the lasing wavelength with respect to the maximum of the gain spectrum (normalized to the gain spectral width); $d_1=\chi/(\pi(1+\Delta^2))$; functions f_i $(i=1,2,3)$ are related to the angular distribution of the excited ions $n(\theta)$ expanded into a Fourier series as follows [17-20]:

$$n(\theta)=\frac{n_0}{2}+\sum_{k=1}^{\infty}n_{1k}\cos(k\theta)+\sum_{k=1}^{\infty}n_{2k}\sin(k\theta),$$

$$f_1=\left(\chi\frac{n_0}{2}-1\right)+\chi\frac{n_{12}}{2},\ f_2=\left(\chi\frac{n_0}{2}-1\right)-\chi\frac{n_{12}}{2},\ f_3=\chi\frac{n_{22}}{2}. \tag{2}$$

Eqs. (2) mean that the dipole moments of the absorption and emission transitions for erbium doped silica are located in the plane orthogonal to the direction of the light propagation. Unlike more general assumption of the 3D orientation distribution of the dipole orientations [20, 21], approximation in the form of Eqs. (2) allows deriving the finite dimension system presented by Eqs. (1) where only n_0, n_{12}, and n_{21} components contribute to the vector dynamics. To analyze conditions for the emergence of RWs we use Stokes presentation of Eqs. (1) through the change of variables:

$$S_0=|v|^2+|u|^2,\ S_1=\left(|u|^2-|v|^2\right),\ S_2=2|u||v|\cos(\Delta\phi),\ S_3=2|u||v|\sin(\Delta\phi). \tag{3}$$

3.2 The theoretical results

We have numerically solved the Eqs. (1) using the following values for the parameters: β=0, α_1=ln(10)6.4, α_2=ln(10)0.5, χ=3/2, Δ=0.1, δ=0.9, γ=2x10^{-6}, ε=10^{-4} and varying the parameter I_p between 19 and 60. The

results for I_p=*19, 20, 23* and *30* are illustrated in Figures 2 – 4. The numerical results of the simulation are summarized in Table 1. In the Table one SWH means significant wave height, the Max(I) and Mean(I) are the maximum and the mean value of the histogram (Figure 3) and η is the likelihood of RW events i.e. the area of under the distribution function on the right side of the RW threshold. As follows from Figures 2A – 4A, the trajectories are located on the circle close to the pole on the Poincare sphere and, though output distribution is non-Gaussian, there are no rogue waves. With increased pump power (Figure 2B-4B, 2C-4C, 2D-4D), trajectories can move between attractors located nearby poles on the Poincare sphere. As follows from Fig. 5C and Table I, residence times nearby attractors reach the maximum asymmetry for I_p=*23* that coincide with the maximum in the percentage of the rogue waves of 0.841%. Finally, in the case of high pump (I_p=*60*) SOP is locked and RWs disappear.

4. THE EXPERIMENTAL RESULTS

4.1 The experimental results near threshold

Since the RW events have low likelihood we took 10 frames of 1024 points each one and then merged the files together. In that way, the whole period of observation was 10 ms. At each point, the polarimeter was integrating the data for 1 μs. The SOP evolution for the different pump slightly exceeding the threshold is illustrated in Figure 7. As seen in the theoretical results, the pattern changed gradually from steady state to form clusters of pulses and then to a noisy regime. The likelihood of RW also behaved like the theoretical predictions. As the pump power is increased, it grows fast beginning from zero (cases A, B and C in Figure 6) and then decreases (compare Table 1 and Table 2). The evolution of the Stokes parameters on the Poincare sphere for the same four cases is illustrated in Figure 7. The spiral-like trajectories were not observed and this can be explained by the long integration time of the polarimeter and by the randomness of the samples obtained. Instead of either conical sections or spiral trajectories we have observed pulsating rings (see case B and C in Figure 7) along with jumps between points on the Poincare sphere. Statistics of the output power is shown in Figure 8. As follows from this figure, rogue waves emergence and suppression with increased pump power follow the theoretical trend shown in Figure 3.

4.2 The experimental results far from the threshold

The upper threshold of pump power was determined by the optical damage we induced in the saturable absorber. The highest value of current we were able to supply to the pump diode without burning a hole in the absorber was ~120 mA. The results we obtained for a pump current of 114.8 mA are illustrated in Figure 9. We have observed that the laser emission was stabilizing, the histogram acquired a Gaussian shape and only one stable attractor was observed on the Poincare sphere. The optical spectrum becomes smooth which implies the absence of abrupt and chaotic oscillations in the system.

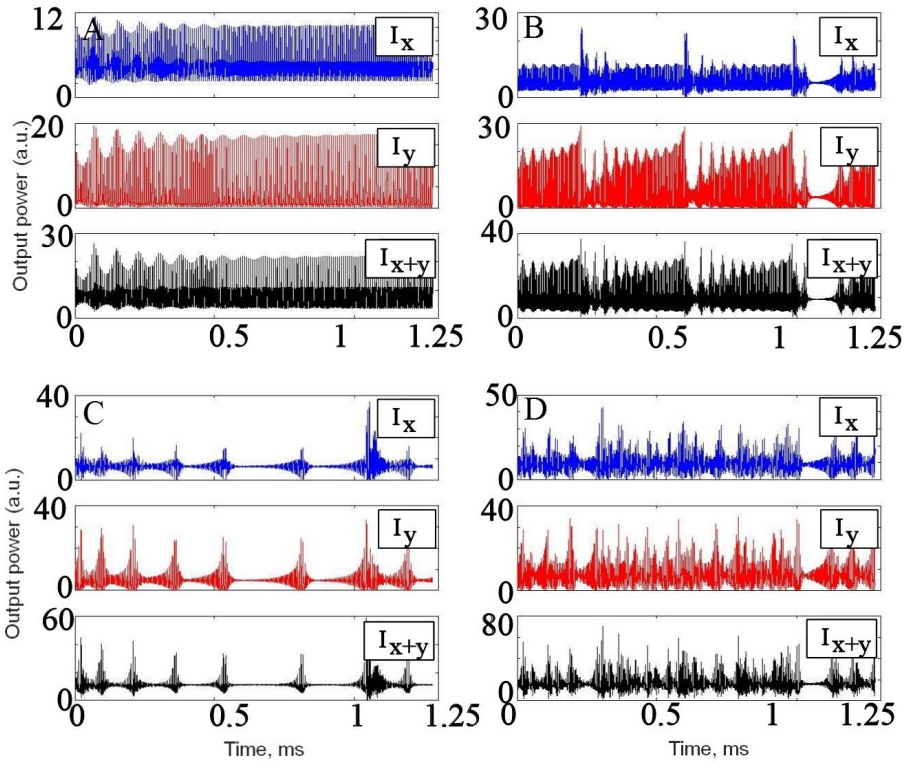

Figure 2. Dynamics of the output power for two orthogonal states of polarization for different pump powers I_p. A) I_p=19, B) I_p=20, C) I_p=23, D) for I_p=30.

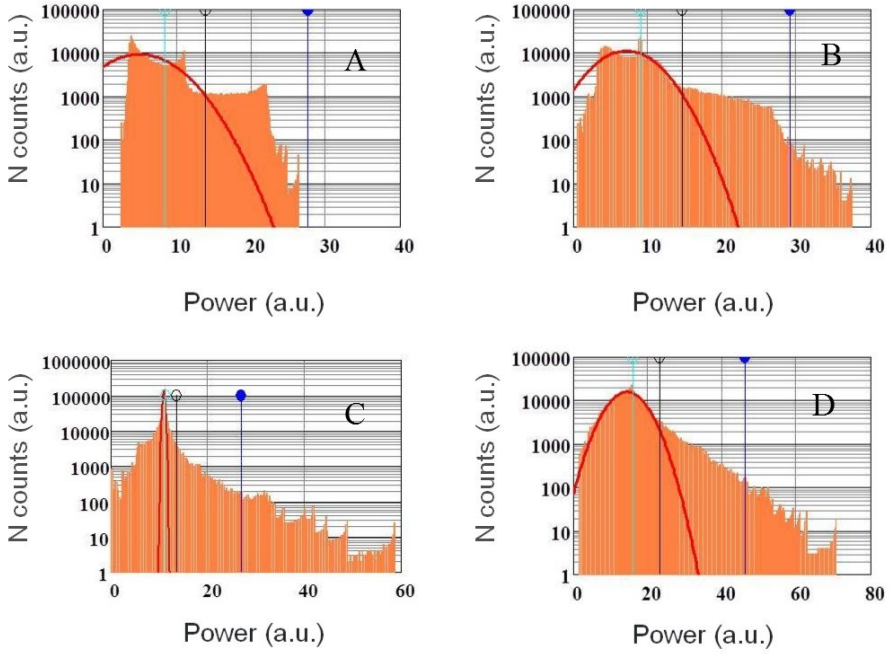

Figure 3. Output power distribution for different pump powers I_p: A) I_p=19, B) I_p=20, C) I_p=23, and D) I_p=30.

Table I. The theoretical results.

I_p, a.u	SWH, a.u	Max(I), a.u	Mean(I), a.u	η (%)
19	13.28	26.345	6.7	0
20	14.574	37.441	9.034	0.209
23	13.418	58.766	11.114	0.841
30	23.093	70.695	15.94	0.432
60	36.736	37.007	36.704	0

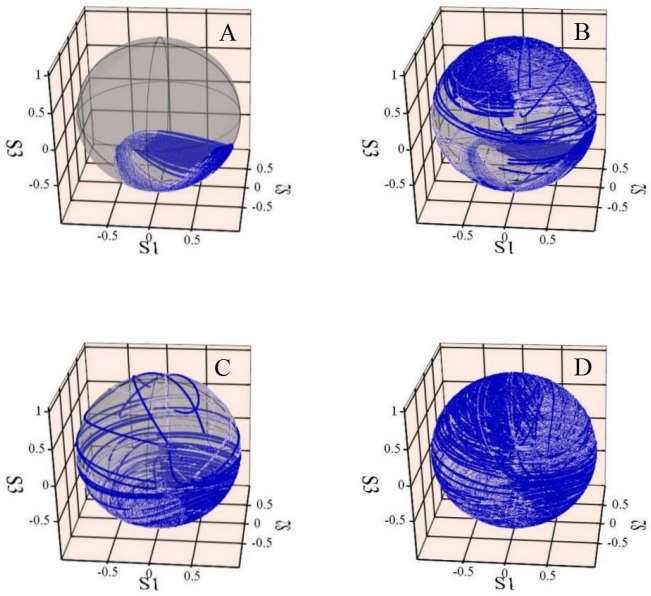

Figure 4. Polarization dynamics represented on Poincare spheres in the case of low pump power: A) I_p=19, B) I_p=20, C) I_p=23, and D) I_p=30.

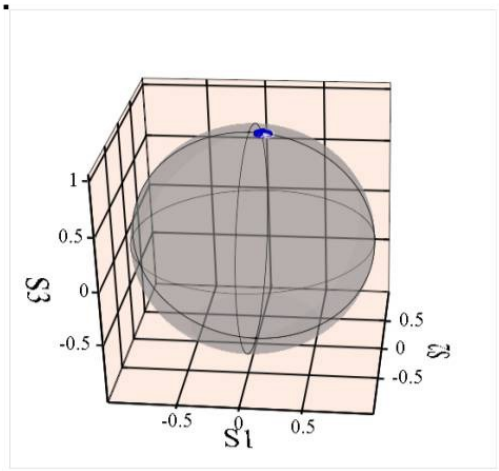

Figure 5. The locked SOP for I_p=60.

5. DISCUSSION

We considered theoretically and experimentally conditions for the emergence of slow rogue waves in mode-locked fiber lasers. This type of rogue waves have a time scale from 20-20000 round trips and is similar to the fluctuation induced escape in asymmetric double well potential [13-16]. The asymmetric potential leads to an increased residence time in the deep well and to the emergence of rare transition events satisfying criteria of rogue waves. Unlike fluctuation induced escape, these transitions in mode-locked fiber laser are caused by polarization instability and leads to chaotic dynamics rather than noise induced stochastic fluctuations. Asymmetry of the potential wells is determined by the increased ellipticity of the pump wave. Accompanied by the increased pump power the asymmetry is increasing that finally results in the transformation of the double well potential into the single well deep potential well and so in polarization locked regime without rogue waves. The observed phenomena could provide a base for advancing lasers in the context of increased output power and access to the variety of previously unexplored waveforms. This work could also influence research on RW dynamics in numerous disciplines beyond the scope of photonics.

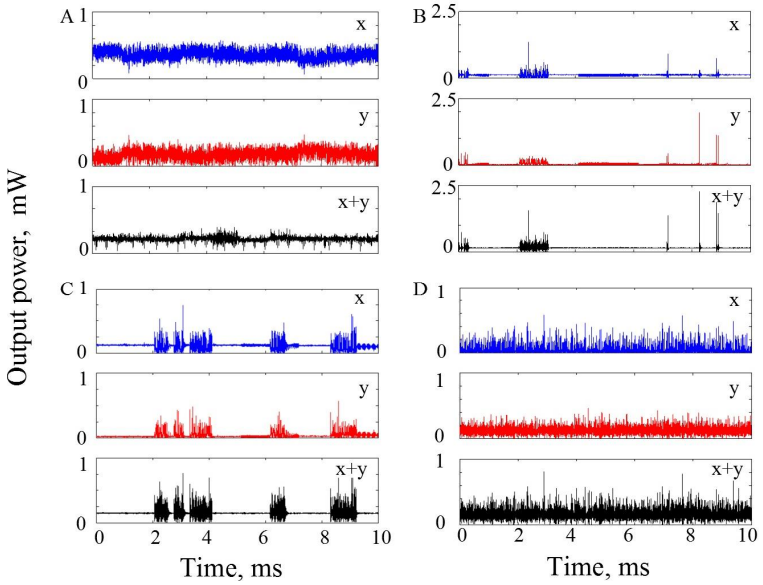

Figure 6. Dynamics of the output power for two orthogonal state of polarization for different pump current i_p; A) i_p=71.2 mA, B) i_p=73.4 mA, C) i_p=74 mA, and D) i_p=75.1 mA.

Table 2. The experimental results.

i_p, mA	SWH, mW	Max(I), mW	Mean(I), mW	η (%)
71.2	0.055	0.064	0.053	0
73.4	0.177	2.278	0.152	0.152
74	0.152	0.685	0.12	0.889
75.7	0.236	0.812	0.155	0.273
114.8	1.321	1.817	1.163	0

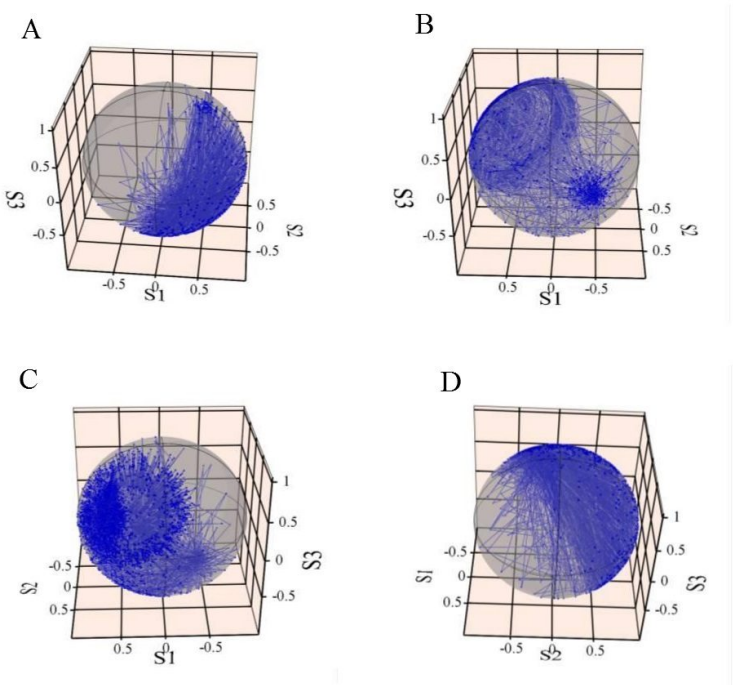

Figure 7. The evolution of the Stokes parameters on the Poincare sphere near the threshold. A) i_p=71.2 mA, B) i_p=73.4 mA, C) i_p=74 mA, and D) i_p=75.1 mA.

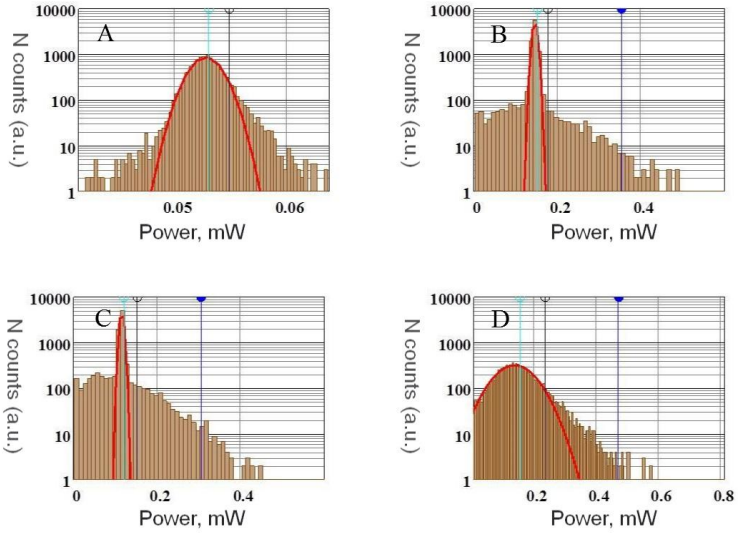

Figure 8. Output power probability distribution near the threshold; A) i_p=71.2 mA, B) i_p=73.4 mA, C) i_p=74 mA, and D) i_p=75.1 mA.

ACKNOWLEDGEMENTS

This work was financed by Leverhulme Trust (Grant ref: RPG – 2014 – 304) and FP7 – 2012 – IAPP (GRIFFON: 324391).

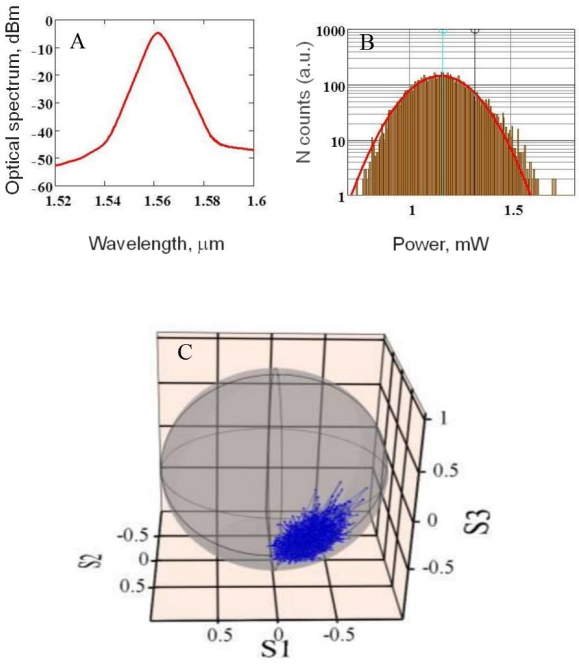

Figure 9. The behavior far from the laser threshold; A_p=114.8 mA.

REFERENCES

[1] Kharif, C., Pelinovsky, E., and Slunyaev, A., "*Rogue Waves in the Ocean*" (Springer, Heidelberg, 2009)

[2] Slunyaev, A., Pelinovsky, E., Sergeeva, A., Chabchoub, A., Hoffmann, N., Onorato, M., Akhmediev, N., "Super-rogue waves in simulations based on weakly nonlinear and fully nonlinear hydrodynamic equations," Physical Review E 88(1), 012909 (2013).

[3] Osborne, A.R. *Nonlinear Ocean Waves and the Inverse Scattering Transform* (Academic Press, 2010).

[4] Zhen-Ya, Y., "Financial rogue waves," Commun. Theor. Phys. 947, 6-9 (2010)

[5] Onorato, M., Residori, S., Bortolozzo, U., Montina, A. & Arecchi, F. T., "Rogue waves and their generating mechanisms in different physical contexts," Phys. Rep. 528, 47 – 89 (2013).

[6] Dudley, J. M., Dias, F., Erkintalo, M., and Genty, G., Instabilities, breathers and rogue waves in optics, Nature Photonics, 8, 755–764 (2014)

[7] Akhmediev, N., Dudley, J. M., Solli, D. R. & Turitsyn, S. K., "Recent progress in investigating optical rogue waves," J. Opt. 15, 060201 (2013).

[8] Lecaplain, C., Grelu, Ph., Soto-Crespo, J. M., Akhmediev, N., "Dissipative Rogue Waves Generated by Chaotic Pulse Bunching in a Mode-Locked Laser," Phys. Rev. Lett. 108 (23), 233901 (2012).

[9] Lecaplain, C., Grelu, Ph., Soto-Crespo, J. M., Akhmediev, N., "Dissipative rogue wave generation in multiple-pulsing mode-locked fiber laser," Journal of Optics 15, 064005 (2013).

[10] Zavialov, A., Egorov, O., Iliev, R., and Lederer, F., "Rogue waves in mode-locked fiber lasers", Phys. Rev. A 85, 013828 (2012).

[11] Donovan, G. M., "Dynamics and statistics of noise-like pulses in modelocked lasers," Physica D 309, 1-8 (2015).

[12] Lecaplain, C., Grelu, Ph, Soto-Crespo, J. M., and Akhmediev, N., "Dissipative rogue wave generation in multiple-pulsing mode-locked fiber laser," J. Opt. 15, 064005 (2013).
[13] Hanggi, P. "Escape from a metastable state," J. Stat. Physics 42, 105-148 (1986).
[14] Lindner, B., Garsia-Ojalvo, J., Neiman, A., Schimansky-Greif, L., "Effects of noise in excitable systems," Phys. Reports 392, 321-424 (2004).
[15] Gammaitoni, L., Hänggi, P., Jung P., and Marchesoni, F., "Stochastic resonance," Rev. Mod. Phys. 70, 223-287(1998).
[16] Armaroli, A., Conti, C., and Biancalana, F., "Rogue solitons in optical fibers: a dynamical process in a complex energy landscape," Optica 2, 497-503 (2015).
[17] Sergeyev, S. V., Mou, Ch., Turitsyna, E. G., Rozhin, A., Turitsyn, S. K., and Blow., K., "Spiral attractors created by vector soliton" Light: Science & Applications 3, e131(2014).
[18] Sergeyev, S. V., "Fast and slowly evolving vector solitons in mode locked fibre laser," Phil. Trans. R. Soc. A 372, 20140006. (2014).
[19] Zeghlache, H., Boulnois, A., "Polarization instability in lasers. I. Model and steady states of neodymium-doped fiber lasers," Phys Rev A 52, 4229-4242 (1995).
[20] Leners, R, Stéphan, G., "Rate equation analysis of a multimode bipolarization Nd^{3+} doped fibre laser," Quantum Semiclass. Opt. 7, 757-794 (1995).
[21] Sergeyev, S. V., "Spontaneous light-polarization symmetry breaking for an anisotropic ring-cavity dye laser," Phys Rev A 59, 3909- 3917 (1999).